

# In-Situ Generation of Maximum Trivalent Cobalt in Synthesis of Hydrotalcite-like Compounds



Z. P. Xu and H. C. Zeng\*

Department of Chemical and Environmental Engineering, Faculty of Engineering,  
National University of Singapore, 10 Kent Ridge Crescent, Singapore 119260

Received January 19, 2000

In-situ generation of trivalent cobalt cations has been investigated for the hydrotalcite-like compounds  $\text{Mg}_x\text{Co}^{\text{II}}_{1-x-y}\text{Co}^{\text{III}}_y(\text{OH})_2(\text{NO}_3)_y \cdot n\text{H}_2\text{O}$  at 25–40 °C under oxygen-containing atmospheres. It is noted that with more involvement of  $\text{Mg}^{2+}$  in the compounds, less  $\text{Co}^{2+}$  cations are needed to maintain the hydrotalcite-like structure. Because of the presence of the  $\text{Mg}^{2+}$ , more  $\text{Co}^{2+}$  can be oxidized under the current experimental conditions and the highest mole ratios of  $\text{Co}^{3+}$  to total cobalt cations ( $\text{Co}^{3+}:\text{Co}$ ) observed in this work is 57%. The mole ratio of  $\text{Co}^{3+}$  to total metal cations ( $\text{Co}^{3+}:(\text{Mg}+\text{Co})$ ) achieved in this work is 31% after 4 days of oxidation reaction, which is close to its upper charge limit to produce a single-phase hydrotalcite-like structure (33%). Two major thermal events are observed when the compounds are heated. The first one at 113–134 °C is attributed to the removal of interlayer water molecules while the second at 274–333 °C to the dehydroxylation and decomposition of intercalated anions. Higher catalytic activity for nitrous oxide ( $\text{N}_2\text{O}$ ) decomposition is observed for the Mg–Co oxides with the same cobalt content but lower mole ratios of  $\text{Co}^{3+}:\text{Co}$  in their hydrotalcite-like precursors. The reason for this activity variation has also been addressed.

## Introduction

In recent years, synthesis of layered double hydroxide materials has become an active field in materials research owing to their many important applications.<sup>1–4</sup> Hydrotalcite-like compounds, in particular, attract much attention in preparing catalyst and ceramic precursors, and in tailoring anion adsorbents, medicine stabilizers, and ion exchangers.<sup>1,5,6</sup>

In this class of compounds, a divalent cation is located in the center of oxygen octahedron formed by six hydroxyl groups. The metal-octahedrons then share their edges to form two-dimensionally infinite sheets, which is similar to the basic structure of brucite  $\text{Mg}(\text{OH})_2$ .<sup>1</sup> These brucite-like sheets can stack to build a three-dimensional network due to the presence of various chemical interactions between the sheets. However, if some of divalent cations in the brucite-like sheets are replaced by the trivalent cations, anions from the solution will then be intercalated into the intersheet space (interlayer space) to maintain charge neutrality for the solid, which leads to the formation of hydrotalcite-like structure (named after natural hydrotalcite compound,  $\text{Mg}_6\text{Al}_2(\text{OH})_{16}\text{CO}_3 \cdot 4\text{H}_2\text{O}$ ).<sup>1</sup>

The layered double hydroxides are commonly prepared using coprecipitation method in basic aqueous solutions.<sup>1</sup> On the basis of chemical composition and structures of desired hydrotalcite-like compounds, syntheses are normally commenced with a predetermined ratio of divalent cations to trivalent cations (normally  $\text{Al}^{3+}$ ) prior to the coprecipitation and the initial cation ratios are generally expected to be the same as in their final solid-phase compounds.<sup>1</sup> It should be mentioned that in this common synthetic approach, the usage of trivalent  $\text{Al}^{3+}$  is indispensable as it is able to provide an extra positive charge (with respect to a divalent cation) to the brucite-like sheets to meet the charge requirement of the hydrotalcite-like structure. Nevertheless, under certain circumstances, such as preparation of hydrotalcite-like precursors for making bimetallic oxides, the inclusion of  $\text{Al}^{3+}$  may not be desirable. To prepare the  $\text{Al}^{3+}$ -free hydrotalcite-like compounds, other trivalent cations such as  $\text{Ga}^{3+}$ ,  $\text{Fe}^{3+}$ ,  $\text{Cr}^{3+}$ , and  $\text{V}^{3+}$  (or occasionally quadrivalent ions such as  $\text{Si}^{4+}$ ,  $\text{Ti}^{4+}$ , and  $\text{Zr}^{4+}$ ) then need to be considered.<sup>1,7–12</sup> Apart from these common trivalent cations that are stable in solutions,

\* Corresponding author. Telephone: +65 874 2896. Telefax: +65 779 1936. E-mail: chezhc@nus.edu.sg.

- (1) Cavani, F.; Trifiro, F.; Vaccari, A. *Catal. Today* **1991**, *11*, 173.
- (2) Reiche, W. T. *Solid State Ionics* **1986**, *22*, 133.
- (3) Faure, C.; Borthomieu, Y.; Delmas, C.; Fonsassier, M. *J. Power Sources* **1991**, *36*, 113.
- (4) Armor, J. N.; Braymer, T. A.; Farris, T. S.; Li, Y.; Petrocelli, F. P.; Weist, E. L.; Kannan, S.; Swamy, C. S. *Appl. Catal. B* **1996**, *7*, 397.
- (5) Hermosin, M. C.; Pavlovic, J.; Ulibarri, M. A.; Cornejo, J. *Water Res.* **1996**, *30*, 171.
- (6) Chisem, I. C.; Jones, W. *J. Mater. Chem.* **1994**, *4*, 1737.

(7) (a) Fuda, K.; Kudo, N.; Kawai, S.; Matsunaga, T. *Chem. Lett.* **1993** (The Chemical Society of Japan) 777. (b) Labajos, F. M.; Rives, V.; Malet, P.; Centeno, M. A.; Ulibarri, M. A. *Inorg. Chem.* **1996**, *35*, 1154.

(8) Hansen, H. C. B.; Koch, C. B.; Taylor, R. M. *J. Solid State Chem.* **1994**, *113*, 46.

(9) Uzunova, E.; Klissurski, D.; Kabbabov, S. *J. Mater. Chem.* **1994**, *4*, 153.

(10) Taylor, R. M. *Clay Miner.* **1984**, *19*, 591.

(11) Boclair, J. W.; Braterman, P. S.; Jiang, J. P.; Lou, S. W.; Yarberr, F. *Chem. Mater.* **1999**, *11*, 303.

(12) Velu, S.; Sabde, D. P.; Shah, N.; Sivasanker, S. *Chem. Mater.* **1998**, *10*, 3451.

some trivalent cations are not stable in aqueous phase but only stable in solid phase. Preparation of trivalent transition metal containing hydrotalcite-like compounds (such as  $\text{MgMn}^{\text{II}}\text{Mn}^{\text{III}}\text{-HT}$ ,  $\text{Ni}^{\text{II}}\text{Mn}^{\text{II}}\text{Mn}^{\text{III}}\text{-HT}$ ,  $\text{Mg}^{\text{II}}\text{Co}^{\text{II}}\text{-Co}^{\text{III}}\text{-HT}$ , and  $\text{Co}^{\text{II}}\text{Co}^{\text{III}}\text{-HT}$ ) has to involve an in-situ oxidation of divalent cations in the solid phase.<sup>13–15</sup> To our knowledge, nonetheless, the investigation on an in-situ generation of trivalent cations is relatively lacking in the field of synthesis of hydrotalcite-like compounds, although it is fundamentally important in terms of solid-state oxidation, relationship, and relative population between the divalent and trivalent cations in the same hydrotalcite-like structures, and chemical properties of the resultant compounds and their derivatives after heat treatment.<sup>16–18</sup>

We had recently synthesized a magnesium–cobalt hydrotalcite-like compound,  $\text{Mg}_{0.3}\text{Co}^{\text{II}}_{0.6}\text{Co}^{\text{III}}_{0.2}(\text{OH})_2(\text{NO}_3)_{0.3}\cdot\text{H}_2\text{O}$ ,<sup>14</sup> in which the trivalent cations  $\text{Co}^{3+}$  were generated during the synthesis via direct oxidation. To test the limit for generation of trivalent cobalt cations, in the current paper, we report a synthesis of a series of Mg,Co-hydrotalcite-like compounds  $\text{Mg}_x\text{Co}^{\text{II}}_{1-x-y}\text{Co}^{\text{III}}_y(\text{OH})_2(\text{NO}_3)_y\cdot n\text{H}_2\text{O}$ . Through insertion of more  $\text{Mg}^{2+}$  into the brucite-like sheets ( $x$  has been increased from 0.3 to 0.6) and prolonged oxidation, we have been able to increase relative mole ratio of  $\text{Co}^{3+}:(\text{Co}^{2+} + \text{Co}^{3+})$  from previous 23% to the current 57% during the in-situ preparation of these compounds, noting that this ratio has reached the upper limit of the charge requirement for a stable single-phase hydrotalcite structure.

### Experimental Section

**Materials Synthesis.** Samples of A1–A5 were prepared by coprecipitation method in ammoniacal solutions. Briefly, 20.0 mL of metal nitrate solution (total cation concentration = 1.0 M;  $\text{Mg}(\text{NO}_3)_2\cdot 6\text{H}_2\text{O}$ , >99.0%, Merck;  $\text{Co}(\text{NO}_3)_2\cdot 6\text{H}_2\text{O}$ , >99.0%, Fluka) with different mole ratio of  $\text{Mg}^{2+}:\text{Co}^{2+}$  was quickly added to 100.0 mL of 0.5 M  $\text{NH}_3\cdot\text{H}_2\text{O}$  solution (Table 1). At the same time, pure  $\text{O}_2$  was introduced by bubbling the solution at 40 mL/min along with rigorous stirring for 18 h. The precipitates were obtained through filtration, washing, and drying in a vacuum overnight. Samples B1, C1, C2, D1, and D2 were prepared in the similar way as for the A1–A5, except a change in aging process. The process parameters included aging time, atmosphere, temperature, and solution alkalinity, which are detailed in Table 1.

**Materials Characterization.** Crystallographic information on the samples of Table 1 was investigated by powder X-ray diffraction (XRD). Diffraction patterns of intensity versus two theta ( $2\theta$ ) were recorded with a Shimadzu XRD-6000 X-ray diffractometer using  $\text{Cu K}\alpha$  radiation ( $\lambda = 1.5418 \text{ \AA}$ ) from  $8^\circ$  to  $42^\circ$  at a scanning rate of  $1^\circ/\text{min}$ . The interlayer spacing of the resultant layered double hydroxides was determined from the diffraction peak positions/patterns with structural analysis software. Chemical bonding information on metal–oxygen, hydroxyl, and intercalated functional groups (such as nitrate anions) were studied with Fourier transform infrared spectroscopy (FTIR, Shimadzu FTIR-8101) using the

**Table 1. Nomenclature of Samples and Synthetic Conditions**

sample	initial mole ratio (mL): $\text{Mg}^{2+}:\text{Co}^{2+}$	ageing time (h)	atmosphere (at 40 mL/min)	$T$ ( $^\circ\text{C}$ )	final pH of filtrate
A1	11:9 (1.2)	18	$\text{O}_2$	25	8.5
A2	14:6 (2.3)	18	$\text{O}_2$	25	8.5
A3	15:5 (3.0)	18	$\text{O}_2$	25	8.5
A4	16:4 (4.0)	18	$\text{O}_2$	25	8.5
A5	17:3 (5.7)	18	$\text{O}_2$	25	8.5
B1	15:5 (3.0)	48	$\text{O}_2$	25	8.5
C1	15:5 (3.0)	48; 48 <sup>a</sup>	$\text{O}_2$ ; air <sup>a</sup>	25; 40 <sup>a</sup>	8.0
C2	15:5 (3.0)	48; 48	$\text{O}_2$ ; air	25; 40	8.5 <sup>b</sup>
D1	15:5 (3.0)	48; 48	$\text{O}_2$ ; air	25; 40	9.5 <sup>c</sup>
D2	15:5 (3.0)	48; 48	$\text{O}_2$ ; air	25; 40	10.0 <sup>d</sup>

<sup>a</sup> In the first 48 h, pure  $\text{O}_2$  was used as an oxidant at  $25^\circ\text{C}$ , and in the second 48 h, pure air was used as an oxidant at  $40^\circ\text{C}$ .

<sup>b</sup> A total of 50.0 mL of 0.5 M  $\text{NH}_3\cdot\text{H}_2\text{O}$  was added at 24 h after coprecipitation. <sup>c</sup> A total of 20.0 mL of 0.5 M NaOH was added at 24 h after coprecipitation. <sup>d</sup> A total of 30.0 mL of 0.5 M NaOH was added at 24 h after coprecipitation.

potassium bromide (KBr) pellet technique. Each FTIR spectrum was collected after 100 scans with a resolution of  $2 \text{ cm}^{-1}$ .

Nitrogen and carbon contents of the prepared samples were measured in a Perkin-Elmer 2400 CHN analyzer, while the magnesium and cobalt contents were determined by ICP measurement (Labtam Plasmascan F10). The trivalent cobalt content was determined by a redox reaction. Typically, 20.00 mg of solid sample was dissolved in 40.0 mL of 1.0 M HCl solution with gentle heating. The produced  $\text{Cl}_2$  gas (from  $\text{Cl}^-$ ) was gradually purged with  $\text{N}_2$  at 40 mL/min and sent to a flask containing 50.0 mL of 0.01 M KI solution mixed with starch indicator. The resultant blue mixture was then titrated against a  $\text{Na}_2\text{S}_2\text{O}_3$  solution (0.0050 M) until the blue coloration disappeared.

Studies with differential thermal analysis (DTA, Shimadzu DTA-50) and thermogravimetric analysis (TGA, Shimadzu TGA-50) were carried out to understand thermal behaviors of the prepared samples. In the DTA/TGA measurements, 15–20 mg of sample was heated respectively at a rate of  $10^\circ\text{C}/\text{min}$  with a flow of air at 40 mL/min over the temperature range of  $40\text{--}500^\circ\text{C}$ . The as-prepared precipitates were also heat-treated at  $400^\circ\text{C}$  for 2 h with static laboratory air in an electric furnace (Carbolite), and their structural phases were then determined by the XRD method (as used in their precursor compounds). Full adsorption–desorption isotherms of nitrogen at  $-196^\circ\text{C}$  for all  $400^\circ\text{C}$  heated samples were measured at various partial pressures in a Quantachrome NOVA-1000 apparatus. Specific surface areas ( $S_{\text{BET}}$ ) and pore-size distributions (PSD) were determined with Brunauer–Emmett–Teller (BET) method and Barrett–Joyner–Hallenda (BJH) method, respectively. BET surface areas were obtained from six adsorption data points in the relative pressure ( $P/P^\circ$ ) range of 0.05–0.35, whereas the PSDs were derived from the desorption isotherms. Prior to  $\text{N}_2$  adsorption measurements, each  $400^\circ\text{C}$  heated sample was degassed with  $\text{N}_2$  purge at  $300^\circ\text{C}$  for 3 h.

In catalytic activity tests, 100 mg of  $400^\circ\text{C}$  heated samples (45–80 mesh) was used in a tubular quartz reactor (inner diameter = 0.4 cm) in each run. In a typical experiment,  $\text{N}_2\text{O}$  gas (1 mol %, balanced with He) was fed at a rate of GHSV =  $20\,000 \text{ h}^{-1}$ . The outlet gases, cooled in a coil, were analyzed by gas chromatography (GC) on a Perkin-Elmer AutoSystem-XL (TCD detector) using a 4-foot Porapak Q (80/100 mesh). The oven temperature of GC was maintained at  $120^\circ\text{C}$ , and the flow rate of carrier gas He was 40 mL/min. The conversion (%) of  $\text{N}_2\text{O}$  to its elementary forms ( $\text{N}_2$  and  $\text{O}_2$ ) was evaluated according to  $X = (P_{\text{N}_2\text{O}} - P_{\text{N}_2\text{O}})/(P_{\text{N}_2\text{O}} + 0.5P_{\text{N}_2}\text{O}P_{\text{N}_2\text{O}})$  where  $P_{\text{N}_2\text{O}}$  and  $P_{\text{N}_2\text{O}}$  are inlet and outlet partial pressures or mole fractions of nitrous oxide.<sup>13c,15b,19</sup>

(20) Moeller, T.; Bailar, J. C., Jr.; Kleinberg, J.; Guss, C. O.; Castellion, M. E.; Metz, C. *Chemistry with Inorganic Qualitative Analysis*; Academic Press: New York, 1990; pp 950–951; p A23.

(13) (a) Fernandez, J. M.; Barriga, C.; Ulibarri, M. A.; Labajos, F. M.; Rives, V. *J. Mater. Chem.* **1994**, *4*, 1117. (b) Barriga, C.; Fernandez, J. M.; Ulibarri, M. A.; Labajos, F. M.; Rives, V. *J. Solid State Chem.* **1996**, *124*, 205. (c) Qian, M.; Zeng, H. C. *J. Mater. Chem.* **1997**, *7*, 493.

(14) Zeng, H. C.; Xu, Z. P.; Qian, M. *Chem. Mater.* **1998**, *10*, 2277

(15) (a) Xu, Z. P.; Zeng, H. C. *Chem. Mater.* **1999**, *11*, 67. (b) Xu, Z. P.; Zeng, H. C. *J. Mater. Chem.* **1998**, *8*, 2499.

(16) Kanazaki, E. *Mater. Res. Bull.* **1998**, *33*, 773

(17) Kanazaki, E. *Solid State Ionics* **1998**, *106*, 279.

(18) Markov, L.; Petrov, K.; Lyubchova, A. *Solid State Ionics* **1990**, *39*, 187.

(19) Wang, X. F.; Zeng, H. C. *Appl. Catal. B* **1998**, *17*, 89.

**Table 2. Chemical Compositions (in mole ratios) of the As-Prepared Precipitates and Coefficients for the Chemical Formula of Hydrotalcite-like Compounds  $Mg_aCo^{II}_bCo^{III}_c(OH)_d(NO_3)_e(CO_3)_f \cdot nH_2O^a$** 

sample	phase	Mg:Co	Co <sup>3+</sup> :Co	Co <sup>3+</sup> :(Co+Mg)	A <sup>-</sup> :(Co+Mg)	a	b	c	d	e	f	n
A1	HT	0.32	0.32	0.24	0.25	0.24	0.52	0.24	1.99	0.17	0.04	0.7
A2	HT	0.63	0.34	0.21	0.23	0.39	0.40	0.21	1.98	0.15	0.04	0.7
A3	HT	1.00	0.38	0.19	0.22	0.50	0.31	0.19	1.97	0.14	0.04	0.7
A4	HT+B	1.33	0.37	0.16	0.20							
A5	HT+B	1.72	0.34	0.13	0.16							
B1	HT	0.91	0.44	0.23	0.30	0.48	0.29	0.23	1.93	0.26	0.02	0.6
C1	HT	0.74	0.51	0.29	0.34	0.43	0.28	0.29	1.95	0.28	0.03	0.7
C2	HT	0.83	0.57	0.31	0.26	0.45	0.24	0.31	2.05	0.22	0.02	0.7
D1	HT	1.21	0.45	0.20	0.23	0.55	0.25	0.20	1.97	0.21	0.02	0.7
D2	HT+B	1.92	0.52	0.18	0.21							

<sup>a</sup> Abbreviations: HT, hydrotalcite-like phase; B, brucite-like phase; Co, Co<sup>2+</sup> + Co<sup>3+</sup>; and A<sup>-</sup>, NO<sub>3</sub><sup>-</sup> + 2CO<sub>3</sub><sup>2-</sup>.

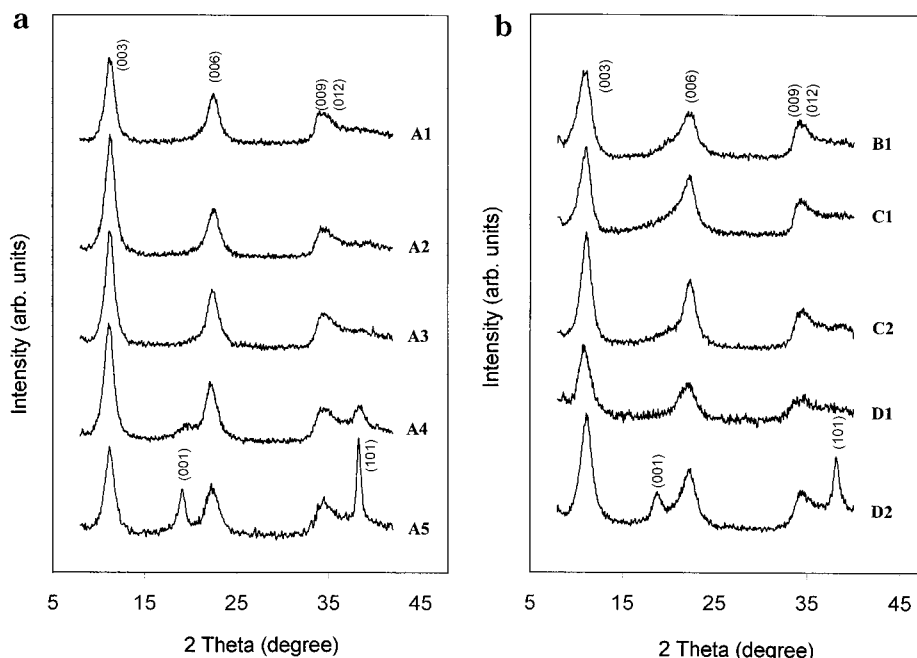


**Figure 1.** XRD patterns of the as-prepared hydrotalcite-like compounds: (a) A1–A5, noting that A4 and A5 contain the brucite-like phase, and (b) B1, C1, C2, D1, and D2, noting that D2 contains the brucite-like phase.

## Results and Discussion

**Considerations of Synthesis.** On the basis of the elemental analysis, several important mole ratios are reported in Table 2 for the precipitates listed in Table 1. Furthermore, chemical formula for single-phase Mg,Co-hydrotalcite-like compounds are derived (Table 2). In view of a substantial difference between  $K_{sp}$  of  $Mg(OH)_2$  ( $K_{sp} = 7 \times 10^{-12}$ ) and  $K_{sp}$  of  $Co(OH)_2$  ( $K_{sp} = 2 \times 10^{-16}$ ),<sup>20</sup> the present experiments were conducted with a high concentration of  $Mg^{2+}$  to avoid staged precipitation. In particular, the sample series of A1–A5 was prepared as a function of the mole ratio of  $Mg^{2+}:Co^{2+}$  in the initial metal solutions (1.2–5.7, Table 1). In this connection, the actual mole ratios of  $Mg^{2+}:Co^{2+}$  in the final precipitates are in the range of 0.32–1.7, which means that only ~30% of original  $Mg^{2+}$  was precipitated out in these experiments (18 h). Among the samples of this series, the A3 gives a highest  $Co^{3+}:Co$  mole ratio of 0.38 (Table 2). To increase the trivalent cobalt in the precipitates, preparation conditions of the A3 were further elaborated in the rest experiments. For example, a longer aging time of 48 h was adopted in the synthesis of B1 sample, which indeed gave a significant increase in the relative content of trivalent cobalt ( $Co^{3+}:Co = 0.44$ , Table 2). A further increase in the mole ratio of  $Co^{3+}:Co$  was achieved with an even longer aging time

(4 days, Table 2) and a gentle heating (40 °C, Table 2) in the experiments of C1, C2, D1, and D2. In the aging process of these samples, the pure oxygen was switched to air which had a lower oxygen partial pressure to prevent the precipitates from a deep oxidation to  $HCoO_2$  inside the solution.<sup>15b,21</sup> In view of the long aging and heating in the C1 experiment, which resulted in a decrease in the final pH value, a supplement of base was also added in C2, D1, and D2 to examine the effect of alkalinity on the synthesis (Table 2). The above synthetic parameters will be further investigated in the following in detail.

**Structural Determination.** The XRD patterns for the precipitates are shown in Figure 1. The peaks at 11.2° (7.89 Å), 22.4° (3.96 Å), and 34.4° (2.61 Å) can be ascribed respectively to the diffractions of the planes of (003), (006), and (009)/(012) of the hydrotalcite-like phase, which is further confirmed with the observation of  $d_{003} = 2d_{006} = 3d_{009}$ .<sup>22a</sup> For the samples of A4, A5, and D2, two extra broad peaks at 19.1° (4.64 Å) and 38.3° (2.35 Å) are also observed, which are assigned to

(21) Furlanetto, G.; Formado, L. *J. Colloid Interface Sci.* **1995**, *170*, 169.

(22) Joint Committee on Powder Diffraction Standards: Swarthmore, PA, 1995; (a) Powder Diffraction File, Card No. 14-0191; (b) Powder Diffraction File, Card No. 45-0031.

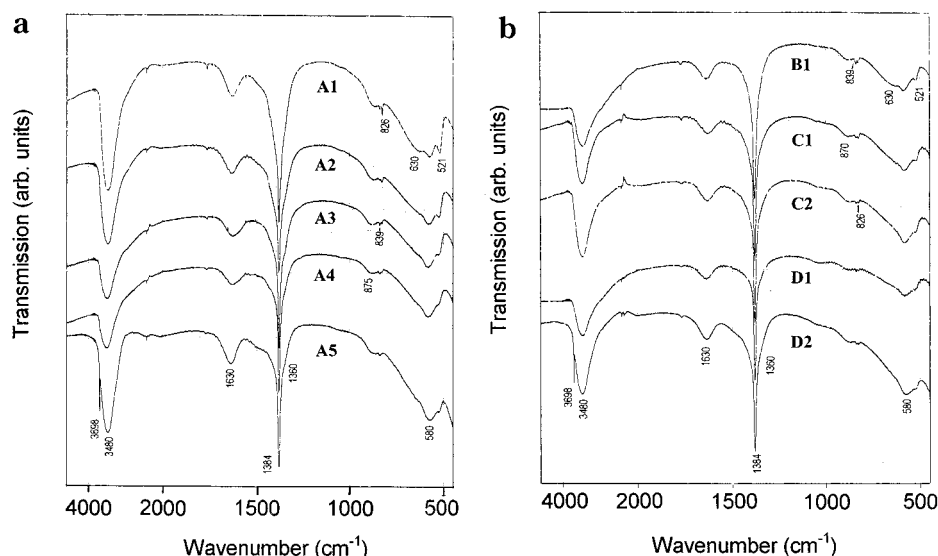


**Figure 2.** FTIR spectra of the as-prepared hydrotalcite-like compounds: (a) A1–A5, noting that A4 and A5 contain the brucite-like phase, and (b) B1, C1, C2, D1, and D2, noting that D2 contains the brucite-like phase.

the diffractions of (001) and (101) planes of the brucite-like phase.<sup>22b</sup> The crystallinity is slightly higher for the samples prepared with a short aging time (18 h, A1–A5), judging from the intensities of the diffraction patterns.

FTIR spectra of the above as-prepared samples are displayed in Figure 2, which further confirms the formation of the hydrotalcite-like phase. The broad band varying from 3450 to 3500  $\text{cm}^{-1}$  is due to OH stretching vibration of the hydroxyl groups of the brucite-like sheets and of intercalated and/or adsorbed water, for which  $\delta_{\text{HOH}}$  is also observed at 1625 to 1635  $\text{cm}^{-1}$ .<sup>6,13,23–25</sup> The intense peak at 1384  $\text{cm}^{-1}$  and a weak shoulder at 1360  $\text{cm}^{-1}$  belong to  $\nu_3$  modes of  $\text{NO}_3^-$  and  $\text{CO}_3^{2-}$  intercalated in the interlayer, which are accompanied by the peaks at 826 and 839  $\text{cm}^{-1}$  due to  $\nu_2$  modes of  $\text{NO}_3^-$  and  $\text{CO}_3^{2-}$  anions.<sup>6,13,24–27</sup> The absence of the peak at 1000–1050  $\text{cm}^{-1}$  ( $\nu_1$  modes,  $D_{3h}$  symmetry)<sup>24</sup> indicates that the two anions are basically unperturbed in the gallery space. Two characteristic bands corresponding to vibrations of hydrotalcite-like phase are located at 583–573 ( $\delta(\text{OH})$ ) and 525–521 ( $\nu(\text{M}-\text{O})$ )  $\text{cm}^{-1}$ , respectively.<sup>13–15</sup> The weak shoulder bands at 880–865 and 630  $\text{cm}^{-1}$ , however, are difficult to assigned with the present experimental conditions, although they may belong to nitrate/carbonate salts ( $\nu_2$  mode for  $D_{3h}$  anions, 880–865  $\text{cm}^{-1}$ ) and lattice vibration (630  $\text{cm}^{-1}$ ).<sup>24</sup>

In good agreement with the XRD results, the presence of brucite-like phase in A4, A5, and D2 samples is reflected in the observation of the OH stretching at 3698  $\text{cm}^{-1}$  in Figure 2. The presence of brucite-like  $\beta\text{-Co}(\text{OH})_2$  in these high-Mg-content samples can be ruled out because the observed wavenumber is exactly the same as that of the pure brucite compound  $\text{Mg}(\text{OH})_2$ <sup>28</sup> which is 68  $\text{cm}^{-1}$  higher than that of OH stretching mode of

$\beta\text{-Co}(\text{OH})_2$ .<sup>15</sup> It should be noted that the formation of  $\text{Mg}(\text{OH})_2$  in the A4 and A5 samples was due to the high concentrations of  $\text{Mg}^{2+}$  in the initial solutions, whereas in D2 sample the  $\text{Mg}(\text{OH})_2$  was formed during the aging when the additional  $\text{OH}^-$  was added. In any case, the secondary phase  $\text{Mg}(\text{OH})_2$  should be formed only in a later stage due to its larger  $K_{\text{sp}}$ .<sup>20</sup>

**Extent of Oxidation.** As reported in Table 2, the formation of hydrotalcite-like compounds involves a partial oxidation of divalent  $\text{Co}^{2+}$  ( $3d^7$ ) to trivalent  $\text{Co}^{3+}$  ( $3d^6$ ).<sup>13c–15,20</sup> In all single-phase hydrotalcite-like samples, the ratios of  $\text{Co}^{3+}:(\text{Co} + \text{Mg})$  agree well with those of  $\text{A}^-(\text{Co} + \text{Mg})$ , which indicates a good balance between the positive charge in the brucite-like sheets and the negative charge in the interlayer space.<sup>1,13c–15</sup> With the increase in Mg content in the A1–A3 samples, the  $\text{Co}^{3+}:\text{Co}$  mole ratio increases monotonically to 38%. With more involvement of  $\text{Mg}^{2+}$ , less  $\text{Co}^{2+}$  cations are needed to maintain a hydrotalcite-like structure, resulting in a higher mole ratio of  $\text{Co}^{3+}:\text{Co}$ . It is clear now that with more inclusion of the  $\text{Mg}^{2+}$ , more divalent  $\text{Co}^{2+}$  can be oxidized into trivalent  $\text{Co}^{3+}$ . This point was further tested along with other process parameters in the experiments of B1, C1, C2, and D1, which produced only the hydrotalcite-like phase. The mole ratio of  $\text{Co}^{3+}:\text{Co}$  could be increased with a longer aging time, although the Mg:Co ratio decreased after the prolonged aging of 48 h which led to a leaching of  $\text{Mg}^{2+}$  from solid phase (note that there was a slight decrease in pH after aging and  $K_{\text{sp}}$  of  $\text{Mg}(\text{OH})_2$  is greater than that of  $\text{Co}(\text{OH})_2$ ). In the C1 and C2 experiments, the aging time was increased to a total of 4 days. As expected, the relative trivalent population ( $\text{Co}^{3+}:\text{Co}$ ) increases with respect to the increases in both aging time and Mg content. In particular, the C2 sample gives a highest mole ratio  $\text{Co}^{3+}:\text{Co} = 57\%$ , noting that the Mg content of C2 is higher than that of the C1 due to the second addition of ammoniacal solution (final pH = 8.5, Table 1). Further increase in the mole ratio of  $\text{Co}^{3+}:\text{Co}$  seems still to be possible. However, we did not further pursue the investigation, as we believe the 4-day aging (C2, 96 h) is already a time-length longer than that for a practical

(23) Kannan, S.; Swamy, C. S. *J. Mater. Sci. Lett.* **1992**, *11*, 1585.

(24) Ehlssissen, K. T.; Delahaya-Vidal, A.; Genin, P.; Figlarz, M.; Willmann, P. *J. Mater. Chem.* **1993**, *3*, 883.

(25) Hernandez-Moreno, M. J.; Ulibarri, M. A.; Rendon, J. L.; Serna, C. *J. Phys. Chem. Miner.* **1985**, *12*, 34.

(26) Busca, G.; Trifiro, F.; Vaccari, A. *Langmuir* **1990**, *6*, 1440.

(27) Zotov, N.; Petrov, K.; Dimitrova-Pankova, M. *J. Phys. Chem. Solids* **1990**, *51*, 1199.

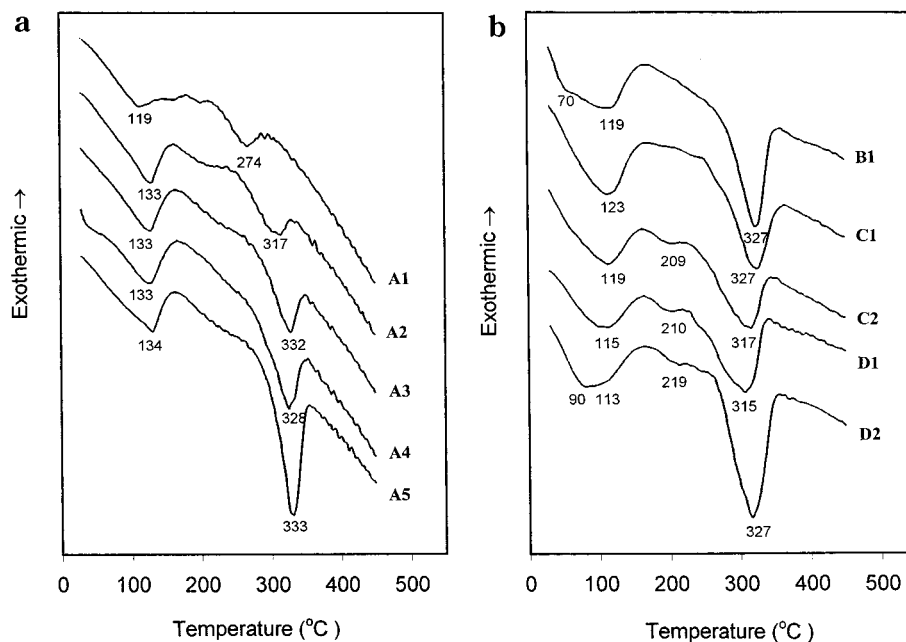


**Figure 3.** DTA scans of the as-prepared hydrotalcite-like compounds: (a) A1–A5, noting that A4 and A5 contain the brucite-like phase, and (b) B1, C1, C2, D1, and D2, noting that D2 contains the brucite-like phase.

synthesis of hydrotalcite-like compounds.<sup>1,13c–15</sup>

In the experiments D1 and D2, the effect of final pH on the oxidation of divalent cobalt was examined via adding NaOH (Table 1) and the final pH values were achieved at 9.5 and 10.0, respectively. It appears that the high pH range is not as suitable for the oxidative formation of hydrotalcite-like compounds as the case of pH = 8.5 (C2), although the contents of Mg can be significantly increased (Mg:Co, Table 2). In fact, the second phase Mg(OH)<sub>2</sub> was formed in D2 sample (final pH = 10.0) noting that the mole ratio of Mg<sup>2+</sup>:Co<sup>2+</sup> in the initial solution was unaltered. Similar secondary phase of Mg(OH)<sub>2</sub> was also found in A4 and A5 when the Mg<sup>2+</sup>:Co<sup>2+</sup> ratio was increased in the initial solutions. As mentioned earlier, the Mg(OH)<sub>2</sub> was only formed after the coprecipitation, which may hamper the oxidation process of the divalent cobalt. Indeed, the crystallinity of Mg(OH)<sub>2</sub> in the A5 sample is higher than that in the A4 (Figure 1) and a lower Co<sup>3+</sup>:Co ratio (34% in the A5 versus 37% in the A4) is thus observed. In this agreement, since crystallinity of Mg(OH)<sub>2</sub> in the D2 sample is not high, the oxidation of divalent cobalt was not affected by the second phase and the trend of Co<sup>3+</sup>:Co ratio was not changed in this set of experiments either.

As demonstrated above, with the careful controls in the synthesis, the relative population of trivalent cobalt has been increased from 23% in our previous work<sup>14</sup> to 57% in the current work. Nevertheless, it should be noted that the absolute contents of trivalent cobalt (Co<sup>3+</sup>:(Co + Mg) or coefficient *c*, Table 2) in the Mg,Co-hydrotalcite-like compounds is increased only from 19% in our previous study to 31% in the current investigation (C2). This observation clearly can be related to chemical and structural requirement in the single-phase hydrotalcite-like compounds that the mole ratio of trivalent cations to total cations is normally in the range of 20% to 33%.<sup>1</sup> The C2 sample therefore represents a Mg,Co-hydrotalcite-like compound which has a content of trivalent cobalt close to its maximum.

**Thermal Decomposition.** The DTA scans of the as-prepared samples are shown in Figure 3, and for all the samples, two distinct thermal events can be observed. The first broad band at 113–134 °C is assigned to the removal of the intercalated water<sup>1,13c,14,15b,29,30</sup> and the shoulders at 70 and 90 °C are due to the dehydration of the physisorbed water on the surface.<sup>30</sup> In the A1–A5 series, the second endothermic band shifts to higher temperatures and becomes more intense as the Mg content in the precipitates increases (Mg:Co, Table 2). These high-temperature thermal events can be attributed to the dehydroxylation and decomposition of intercalated anions of the precipitate compounds/mixtures,<sup>13–17</sup> i.e., the collapse of the layered structures. The high-temperature shifts are understandable since the brucite-like sheets will be thermally more stable if more Mg<sup>2+</sup> cations are incorporated. The upper limit for this stabilizing effect seems to be at Mg:Co = 1, because the dehydroxylation occurred at similar temperatures when the Mg:Co ratio is around 1 (A3–A5, B1, C1, C2, D1, and D2, Table 2). It is worthy pointing out that there was no obvious endothermic peak corresponding to the decomposition of the brucite phase that had been detected in the samples of A4, A5, and D2. This observation indicates that the hydrotalcite-like compounds with high content Mg are very stable.<sup>13c,14</sup>

The above thermal event assignments indeed are in good agreement with TGA investigation (see weight loss data: WL1, WL2, WL3, Table 3). As shown in Figure 4 for the A1–A5 samples, the first and second thermal events detected with DTA are also reflected in the first-order derivative peaks of TGA at the similar temperatures, which correspond to the rapid and large weight losses of the samples upon heating. The small dips at 222–255 °C that are more difficult to be recognized in DTA (209–219 °C, Figure 3) can be related to the partial

(28) Bensi, H. A. *J. Chem. Phys.* **1959**, *30*, 852.

(29) Yun, S. K.; Pinnavaia, T. J. *Chem. Mater.* **1995**, *7*, 348.

(30) Pesic, L.; Salipurovic, S.; Markovic, V.; Vucelic, D.; Kagunya, W.; Jones, W. *J. Mater. Chem.* **1992**, *2*, 1069.

**Table 3. Physical Properties and Catalytic Activities for Some Selected Samples in Decomposition Reaction of N<sub>2</sub>O**

precursor sample	precursor phase	weight loss <sup>a</sup>	oxide phase <sup>b</sup>	S <sub>BET</sub> <sup>c</sup> (m <sup>2</sup> /g)	Co:(Mg+Co) <sup>d</sup> (mol:mol)	conversion <sup>e</sup> (%)	activity <sup>f</sup> (mmol/g·h)	activation energy <sup>g</sup> (kJ/mol)
A1	HT	11.0%; 8.0%; 13.0%	S	129	0.75	70	6.2	103
A3	HT	11.0%; 8.0%; 15.5%	S	136	0.50	49	5.0	106
A5	HT+B	10.0%; 7.0%; 18.0%	S	108	0.38	44	5.5	105
B1	HT	10.5%; 8.0%; 20.0%	S	110	0.52	32	2.1	93
D1	HT	12.0%; 7.0%; 21.0%	S	146	0.45	37	2.9	100
D2	HT+B	11.0%; 7.0%; 21.5%	S	120	0.34	26	2.0	110

<sup>a</sup> Weight loss (WL) data corresponding to the three major thermal events (Figures 3 and 4) in air in sequence of WL1 (40–180 °C), WL2 (180–250 °C), and WL3 (250–500 °C). <sup>b</sup> Structural phase of oxide catalysts derived from their respective precursor compounds at 400 °C for 2 h in static air; S = cubic spinel phase. <sup>c</sup> Specific surface areas of the oxide catalysts derived from their respective precursor compounds at 400 °C for 2 h. <sup>d</sup> Atomic ratio of Co content to total metal content in the oxide catalysts. <sup>e</sup> Conversion data ( $X$ ) were collected for the N<sub>2</sub>O (1 mol %) decomposition at reaction temperature 400 °C. <sup>f</sup> Activity is ascribed as decomposition of N<sub>2</sub>O (in mmol) over 1 g of 400 °C derived catalyst within 1 h of experiment. <sup>g</sup> Activation energies were calculated according to a rate-law of  $r = kP_{N_2O}^{1.5b,19}$  using the data reported in Figure 5.

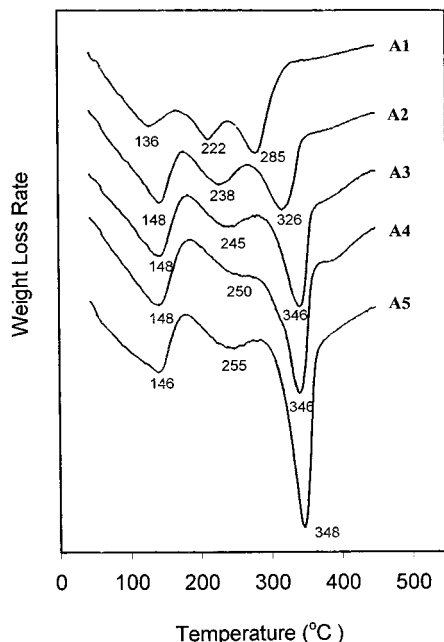


**Figure 4.** DrTGA data of the as-prepared hydrotalcite-like compounds A1–A5, noting that A4 and A5 contain the brucite-like phase.

decomposition of some intercalated anions. These anions may directly attach to the Co cations upon the thermal heating and hence require less thermal energy to decompose,<sup>31</sup> noting that the weight losses here are nevertheless small (WL2, Table 3) and the decomposition temperatures are indeed increased when Co cations are lessened.

**Evaluation of Catalytic Activity.** Compared to the pure cobalt oxides,<sup>15b,32</sup> the specific surface areas  $S_{BET}$  of the calcined samples (spinel phase formed at 400 °C) in this work are much higher, as reported in Table 3. This observation can be attributed to the stabilizing effect of Mg<sup>2+</sup> in the brucite-like sheets, which delays the dehydroxylation to higher temperatures. For the series of A1–A5 and D1–D2, the spinel oxides derived from single-phase hydrotalcite-like compounds have high surface areas (A1, A3, and D1), whereas when Mg(OH)<sub>2</sub> forms as a separated phase in the precursor compounds, there is a drop in  $S_{BET}$  observed in the oxide samples derived from A5 and D2 (Table 3). The oxide

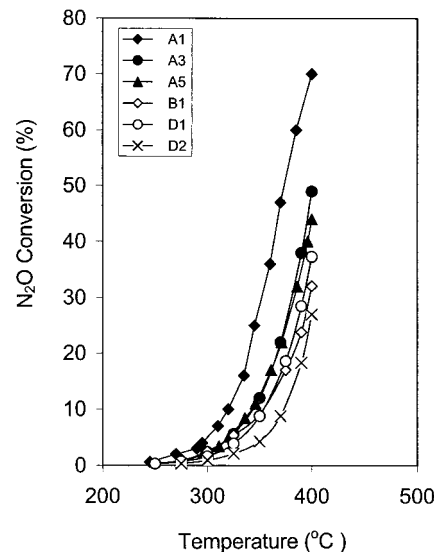


**Figure 5.** Curves of conversion percentage ( $X$ ) versus reaction temperature for spinel catalysts prepared from some selected samples, A1, A3, A5, B1, D1, and D2 (heat-treated at 400 °C for 2 h); catalyst weight used in the flow reactor, 100 mg, and N<sub>2</sub>O (1 mol %) feed rate at GHSV = 20 000 h<sup>-1</sup> under normal atmosphere.

sample derived from B1, however, cannot be compared with the two sample series because the preparative parameters of B1 were uniquely selected (see Tables 1 and 3).

The catalytic activity for N<sub>2</sub>O decomposition is reported in Figure 5. As can be noted, at 250–300 °C, the decomposition reaction starts ( $X = 2$ –4%, 300 °C), and at 400 °C, the conversion is up to  $X = 30$ –70%, indicating they are active catalysts for N<sub>2</sub>O decomposition. The catalyst derived from the A1 compound has the highest conversion ( $X = 70\%$ ) among all the samples (Table 3), noting that it has the highest Co:(Mg + Co) ratio. The high conversion can be attributed to the high content of the cobalt cations, as cobalt has been recognized to be the active species for catalytic decomposition of N<sub>2</sub>O.<sup>15b,33–36</sup> For comparison, hysteresis loops for the most active oxide catalyst derived from A1 and the least active from D2 are plotted together in Figure 6. The two samples give two types of hysteresis loop H1 (porous materials with regular array of particle agglomerates)

(31) Xu, Z. P.; Zeng, H. C. *Chem. Mater.*, revised paper submitted in May 2000.

(32) Mutuberrria, I. G.; Guil, J. M.; Paniego, A. R. *Ber. Bunsen-Ges. Phys. Chem.* **1993**, *97*, 77.

(33) Drago, R. S.; Jurczyk, K.; Kob, N. *Appl. Catal. B* **1997**, *13*, 69.

(34) Cimino, A.; Pepe, F. *J. Catal.* **1972**, *25*, 362.

(35) Cimino, A.; Indovina, V. *J. Catal.* **1970**, *17*, 54.

(36) Chellam, U.; Xu, Z. P.; Zeng, H. C. *Chem. Mater.* **2000**, *12*, 650.

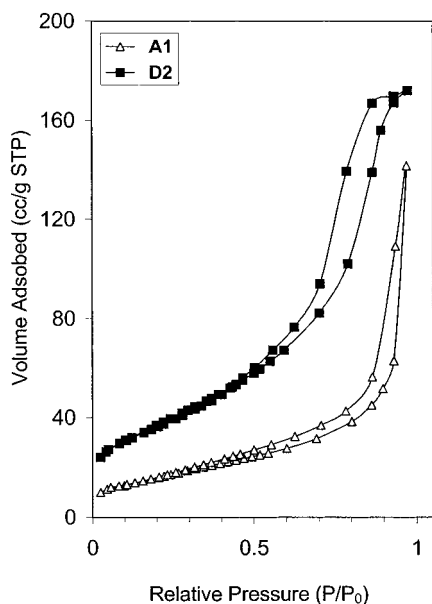


**Figure 6.** Representative nitrogen adsorption-desorption isotherms measured for A1 and D2 samples calcined at 400 °C (in static air) for 2 h.

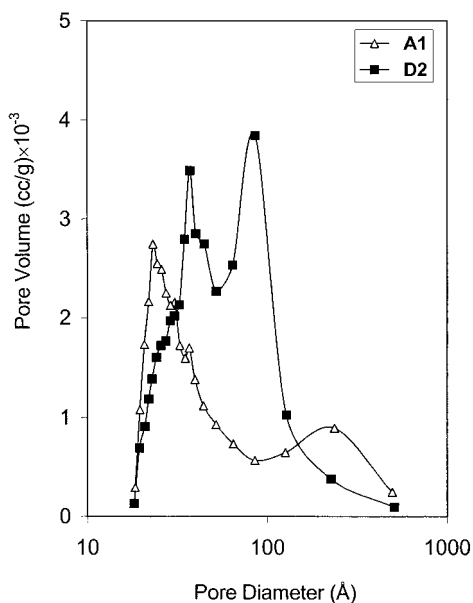


**Figure 7.** Representative pore size distribution profiles (BJH method) measured for A1 and D2 samples calcined at 400 °C (in static air) for 2 h.

and H3 (aggregates often associated with slit-shaped pores), respectively.<sup>37</sup> In this agreement, in Figure 7, the pore-size distributions derived from desorption data show that there is only a main peak centered at 23 Å (and small one at 237 Å) for A1 catalyst while there are two main peaks at 37 and 86 Å respectively for D2, revealing a significant variation in pore structure. It is interesting to note that although the mole ratio of Co:(Mg + Co) in B1 and D1 is similar to that of A3 (noting that surface areas of the three heated samples are also in the similar order, Table 3), their conversion values

are substantially different. Because of longer aging time and thus more oxidation of  $\text{Co}^{2+}$  to  $\text{Co}^{3+}$  in the preparations of B1 and D1, the  $\text{Co}^{3+}:\text{Co}$  ratio in these Mg,Co-hydrotalcite-like compounds is higher ( $\text{Co}^{3+}:\text{Co}$ , Table 2). It has been recognized that the transformation of layered Mg,Co-hydroxides to oxide spinels upon heating is a topotactic process,<sup>18,36,38</sup> especially at a low heating temperature. After heat treatment, some of the divalent  $\text{Co}^{2+}$  have to be further oxidized (by oxygen) to trivalent  $\text{Co}^{3+}$ , producing spinel oxides  $\text{Mg}_x\text{Co}_{3-x}\text{O}_4$  in which the mole ratio of divalent cations to trivalent cations is 1:2.<sup>36,38,39</sup> Since the precursor sample A3 has an originally low  $\text{Co}^{3+}:\text{Co}$  ratio and more  $\text{Co}^{2+}$  need to be oxidized, we believe that the degree of inversion of the resultant spinel upon the thermally oxidative decomposition may be higher in this sample,<sup>18,36,38,39</sup> which leads to higher activity for  $\text{N}_2\text{O}$  decomposition, in particular, the charge-transfer ability (or, electron donation ability) to an adsorbed  $\text{N}_2\text{O}$ .<sup>36</sup> On the contrary, since the  $\text{Co}^{3+}:\text{Co}$  ratios in the precursor compounds of B1 and D1 are higher and less  $\text{Co}^{2+}$  need to be oxidized, the originally formed  $\text{Co}^{3+}$  may be well retained in the octahedron sites, resulting in a lower degree of inversion. As for the D2 sample, the conversion of  $\text{N}_2\text{O}$  decomposition is low, since its Co:(Mg + Co) is the lowest and the active catalyst component for the reaction is accordingly the least.<sup>34,35</sup>

### Conclusions

In summary, the hydrotalcite-like compounds of  $\text{Mg}_x\text{Co}^{\text{II}}_{1-x-y}\text{Co}^{\text{III}}_y(\text{OH})_2(\text{NO}_3)_z \cdot n\text{H}_2\text{O}$  with high content of trivalent cobalt cations can be prepared in-situ at 25–40 °C under oxygen containing atmospheres. When the population of  $\text{Mg}^{2+}$  in the compounds is increased, less  $\text{Co}^{2+}$  cations will be needed to maintain the hydrotalcite-like structure and more  $\text{Co}^{2+}$  can be oxidized to trivalent state under the current experimental conditions. The highest mole ratio of  $\text{Co}^{3+}$  to total cobalt cations ( $\text{Co}^{3+}:\text{Co}$ ) observed in this work is 57% and the mole ratio of  $\text{Co}^{3+}$  to total metal cations ( $\text{Co}^{3+}:(\text{Mg} + \text{Co})$ ) achieved in this work is 31% after 4 days of oxidation reaction, noting that the value is already close to the upper limit of trivalent to total cation ratio to produce a single-phase hydrotalcite-like structure (33%). When these hydrotalcite-like compounds are heated in air, two major thermal events can be observed. The first endothermic peaks at 113–134 °C can be commonly assigned to the removal of interlayer water molecules while the second one at 274–333 °C to the dehydroxylation and decomposition of intercalated anions. Higher catalytic activity for nitrous oxide ( $\text{N}_2\text{O}$ ) decomposition observed for the Mg–Co spinel oxides with the same cobalt content but lower mole ratios of  $\text{Co}^{3+}:\text{Co}$  in their hydrotalcite-like precursors can be explained in terms of variation in degree of inversion of spinel phase upon the aging (solid-state oxidation within the solution) and the direct thermal oxidation in air when the hydrotalcite-like compounds with low  $\text{Co}^{3+}:\text{Co}$  are converted to the spinels.

**Acknowledgment.** The authors gratefully acknowledge research funding (RP3999902/A and A/C50384) cosupported by the Ministry of Education and the National Science and Technology Board of Singapore.

(37) Sing, K. S. W.; Everett, D. H.; Haul, R. A. W.; Moscou, L.; Pierotti, R. A.; Rouquerol, J.; Siemieniowska, T. *Pure Appl. Chem.* **1985**, *57*, 603.

(38) Markov, L.; Lyubchova, A. *J. Mater. Sci. Lett.* **1991**, *10*, 512.

(39) Markov, L.; Petrov, K.; Rachev, P. *React. Solid* **1987**, *3*, 67.